Journal of Catalysis 262 (2009) 134–143

Contents lists available at ScienceDirect

Journal of Catalysis

www.elsevier.com/locate/jcat

# Dehydration of butanol to butene over solid acid catalysts in high water environments

Ryan M. West, Drew J. Braden, James A. Dumesic *

*University of Wisconsin–Madison, Department of Chemical and Biological Engineering, Madison, WI 53706, USA*

ARTICLE INFO

*Article history:*
Received 28 August 2008
Revised 12 December 2008
Accepted 16 December 2008
Available online 22 January 2009

*Keywords:*
2-Butanol
Dehydration
Water
Aqueous phase processing
Silica-alumina
Niobium phosphate
Niobic acid
Butene

ABSTRACT

The effects were studied of high water concentrations on the kinetics of alcohol dehydration, as encountered in aqueous-phase processing of biomass-derived oxygenated hydrocarbons. These studies were carried out for dehydration of an aqueous solution of 10 wt% 2-butanol at 513 K, and at a total pressure of 52 bar to maintain the water in the liquid state. Under these high pressures of water, silica-alumina, niobium phosphate and niobic acid are found to be stable and active for the dehydration of butanol. These three catalysts showed an increase in rate after contact with liquid water, caused by an increase in the concentration of Brønsted acid sites. Zeolite catalysts (Beta, USY, H-ZSM-5) and zirconia based catalysts ($WO_x/ZrO_2$, $MoO_x/ZrO_2$, and $MgO/ZrO_2$) were ineffective due to deactivation or low catalytic activity. The flow rate of inert gas at constant aqueous flow rate had a significant effect on the rate of butene production, due to vaporization of butanol and water. At low flow rates of gas, increasing the gas flow rate causes the preferential vaporization of butanol, leading to a decrease in the butanol pressure in the reactor and a corresponding decrease in the rate of dehydration. Above a critical gas flow rate, the liquid feed becomes completely vaporized in the reactor, and increasing the gas flow rate further leads to a decrease in the pressure of water and a corresponding increase in the rate of dehydration. In the vapor–liquid equilibrium regime, kinetic models predict that most of the catalyst is covered with multiple layers of water, and dehydration takes place by reaction of hydrated–adsorbed butanol with a hydrated surface site. In the vapor-only regime, kinetic models suggest that the fraction of vacant active sites increases with increasing gas flow rate, and dehydration takes place by reaction of adsorbed butanol with a vacant surface site.



## 1. Introduction

Renewable sources for fuels and chemicals must be developed as reserves of non-renewable petroleum feed stocks diminish, and biomass resources are promising alternatives to meet these demands. Considerable research has focused on sugars obtained from biomass, such as fructose and glucose, and their derivatives such as sorbitol [1–5]. Carbohydrates contain high extents of oxygenated functional groups that must be selectively removed or modified to create desired products. These oxygenated groups lead to high solubilities of carbohydrates in water, requiring aqueous-phase processing of these compounds to fuels and chemicals.

A particularly useful reaction sequence for aqueous-phase processing is dehydration followed by hydrogenation, in which oxygenated hydrocarbons, such as sorbitol, are first dehydrated over solid acid sites followed by hydrogenation to form alkyl species. Sequential operation of aqueous-phase dehydration/hydrogenation (APDH) leads to the formation of straight-chain alkanes, such as butane, pentane and hexane [3]. Olefinic species are not typically observed during APDH processing at temperatures near 520 K and pressures near 50 bar over catalysts consisting of Pt (e.g., 4 wt%) supported on acidic supports, such as silica-alumina or niobium phosphate [3,4], suggesting that dehydration is the rate limiting step. In the present paper, we report results of reaction kinetics studies of dehydration reactions over various solid acids catalysts in the presence of liquid water as well as water vapor. Sec-butanol was chosen as the reactant for studies of aqueous-phase dehydration, because it readily undergoes intramolecular dehydration to form butene products. To ensure that dehydration was, in fact, the rate limiting step in APDH processing, 2-butanol was converted to butane over the same Pt/silica-alumina catalyst used in our previous work [3], and 2-butanol was also converted to butenes over the silica-alumina support under the identical reaction conditions. The rates of production of butane and butenes were the same on these two catalysts, indicating that dehydration was indeed the rate limiting step.

Butanol dehydration to butenes has been studied by various authors under conditions involving water. For example, it has been

* Corresponding author.
*E-mail address:* dumesic@engr.wisc.edu (J.A. Dumesic).

0021-9517/$ – see front matter 
doi:10.1016/j.jcat.2008.12.009

reported that water vapor can either increase or inhibit 2-butanol dehydration over zirconia-supported tungsten and silicon based solid acids [6]. A decrease in the activity of $WO_3/ZrO_2$ in the presence of water was investigated by others [7]. However, the performance of solid acid catalysts has not been studied systematically for a wide range of water concentrations, especially high water concentrations and in the presence of liquid water.

## 2. Experimental

### 2.1. Catalysts

Silica-alumina, MCC 25 (SiAl), was obtained from Grace Davidson with a Si/Al ratio of 4. Beta-zeolite with a Si/Al ratio of 25 and USY-zeolite with a Si/Al ratio of 5 [8] were obtained from Engelhard and calcined at 773 K before use. H-ZSM-5 catalyst with a Si/Al ratio of 14 was obtained from Engelhard. Tungstated-zirconia, XZO1251/01 16% $WO_3$, was obtained from MEI Chemicals. $MoO_x/ZrO_2$, with 20.3% $MoO_3$, was prepared in a similar manner as reported in the literature [9], by incipient wetness impregnation of $(NH_4)_6Mo_7O_{24}{\cdot}H_2O$ (Aldrich) on $ZrO_2$ XZO 880/01 purchased from MEI Chemicals. The impregnated solids were dried overnight in air and then treated in a flowing gas mixture of 20% $O_2$ in He at 723 K. $MgO/ZrO_2$ was prepared as detailed elsewhere [10,11]. Niobic acid, HY-340 ($Nb_2O_5$), was obtained from CBMM in Brazil. Niobium phosphate ($NbOPO_4$) was prepared in a similar manner to previous reports [12]. Briefly, 4 g of $NbCl_5$ was reacted 1:2 with phosphoric acid. After thorough mixing, the resulting paste was diluted in 70 mL water and stirred for 40 min. The pH was then adjusted to 4.9 and the mixture was stirred for an additional 30 min. The $NbOPO_4$ was then filtered and washed until the silver nitrate test showed no additional $Cl^-$ ions. The catalyst was dried overnight in air and then treated in a flowing gas mixture of 20% $O_2$ in He at 723 K.

For characterization purposes, SiAl, $Nb_2O_5$ and $NbOPO_4$ were additionally modified to study the effect of liquid water on acidity. In this treatment, approximately 0.5 g of catalyst was placed in a glass beaker with 50 mL of water. The beaker was placed in a sealed Parr reactor and heated to the reaction temperature of 513 K for 3 h. The reactor was cooled, the water was decanted, and the catalyst was then placed in an oven overnight to dry at 393 K.

### 2.2. Reactor setup

Catalysts were mixed with crushed silica and packed with quartz wool end-plugs in tubular quarter-inch stainless steel reactors. Except where noted otherwise, a ten weight percent solution of 2-butanol (Aldrich) in deionized water was fed with an HPLC pump in an up-flow direction over the catalyst bed. The effluent was collected in a gas–liquid separator. Inert gas (He or $H_2$ from Linde) was flowed through the catalyst bed by means of a mass flow controller, and this flow was used to control the water concentration within the reactor. In addition, inert gas was flowed though the separator to direct gaseous species to a gas chromatograph for on-line analysis. The pressure of the system was held constant at 52 atm by a back pressure regulator. The reactor was held at a constant temperature of 513 K as measured by a thermocouple attached to the exterior of the reactor and surrounded by aluminum blocks within an oven. The effluent gas was analyzed by an online GC, Varian GC-MS (Saturn 3) using an FID detector and a GS-Q capillary column (J&W Scientific). The liquid effluent was collected and analyzed by a Shimadzu GC2010 equipped with an FID detector and a DB 5 ms column (J&W Scientific). Total carbon material balances on individual points typically closed within 5%.

In a typical experimental run, the reactor was heated to the reaction temperature while inert gas was flowed over the catalyst. After reaching the reaction temperature, the inert gas was flowed for an additional hour before introducing the butanol/water mixture. After changing conditions, the system was allowed a minimum of 5 h to reach steady state before sampling the phases.

### 2.3. Catalyst characterization

The surface areas of all catalysts were determined from BET isotherms of $N_2$ adsorption at 77 K. The concentration of acid sites per gram of each catalyst was quantified by temperature programmed desorption of ammonia. Catalyst samples (~100 mg) were loaded into a glass flow through cell, ammonia was adsorbed onto the catalyst for 1.5 h at room temperature, physically adsorbed ammonia was then desorbed at 423 K, and TPD experiments commenced using a temperature ramp of 10 K/min. The desorbed ammonia was quantified on-line using a mass spectrometer.

The distribution of Brønsted and Lewis acid sites was determined from infrared measurements of adsorbed pyridine. Approximately 10 mg of catalyst was placed in a 1.2 cm dye and pressed into a pellet, which was then placed in a treatment/sampling cell where it was heated to 473 K under flowing dry $N_2$ (Linde) for 2 h. A reference spectrum of the catalyst was then taken. Pyridine was introduced into the cell for 30 min at room temperature, followed by heating at 473 K overnight under flowing dry $N_2$. The areas of the pyridine peaks at 1455 and 1545 $cm^{-1}$ (Lewis and Brønsted sites, respectively) were then determined by subtracting the spectra of the sample before and after this exposure to pyridine.

### 2.4. Methods

The activity of each catalyst was tested under the same reaction conditions, consisting of a flow equal to 0.1 mL/min of feed solution (10 wt% butanol in water) and a gas flow of 200–215 $cm^3$(STP)/min. After this initial screening, the three zirconia-based catalysts, $MgO/ZrO_2$, $WO_x/ZrO_2$, and $MoO_x/ZrO_2$ were eliminated from further investigation, because the rates of butene production for these three catalysts were 1.3, 2.6 and 5.3 μmol/g/min, respectively; these values are an order of magnitude lower than the activities of the other catalysts. Beta-zeolite was also removed from further consideration, because although it initially demonstrated a high rate of butene production (1600 μmol/g/min), it showed a continual decrease in activity under the reaction conditions of this study, as shown in Fig. 1.

The rates of dehydration of the remaining five catalysts are shown in column 1 of Table 1. H-ZSM-5 and USY showed the highest rates of 2403 and 962 μmol/g/min, respectively. SiAl, $Nb_2O_5$

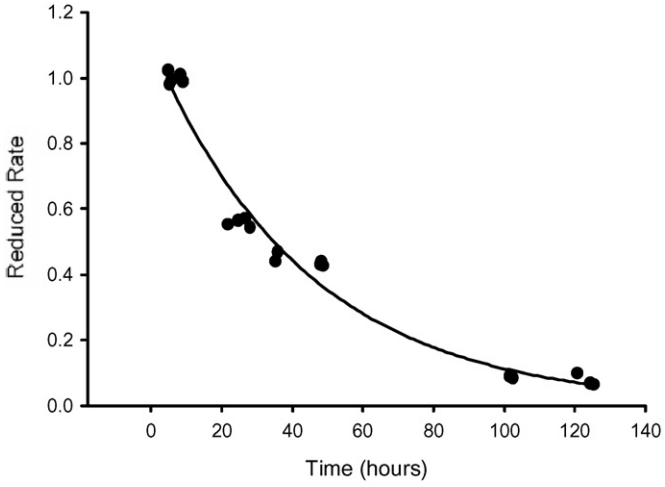


**Fig. 1.** Normalized rate versus time on stream in high water environment for Beta-zeolite.

**Table 1**
Reactivity and properties of solid acid catalysts for the dehydration of 2-butanol in aqueous media.

| | Rate at 200–215 $cm^3$(STP)/min of He (μmol/min g cat) | Rate after exposure to liquid water (μmol/min g cat) | Acid site density (μmol/g)[a] | Brønsted area/Lewis area[a] | BET surface area ($m^2$/g)[a] |
|---|---|---|---|---|---|
| SiAl | 153 | 181 | 578/756 | 0.15/12.5 | 498/169 |
| $NbOPO_4$ | 81 | 262 | 265/536 | 2.6/2.1 | 185/85 |
| $Nb_2O_5$ | 40 | 147 | 135/22 | 1.1/3.0 | 118/17 |
| H-ZSM-5 | 2403 | 1373 | 542/– | 20.7/– | –/– |
| USY | 962 | 315 | 1015/– | 9.6/– | –/– |

[a] Untreated catalyst/water treated catalyst.

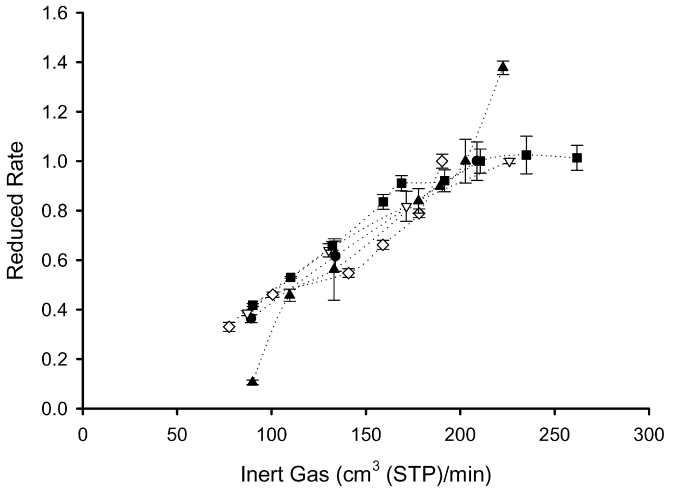


**Fig. 2.** Normalized rate (rate at given He flow rate/ flow rate at 200–215 $cm^3$(STP)/min) versus inert gas flow rate. SiAl (■); $Nb_2O_5$ (●); $NbOPO_5$ (▽); H-ZSM-5 (◇); USY (▲).

and $NbOPO_4$ all had similar rates of 153, 40, and 81 μmol/g/min, respectively.

At constant liquid flow of 0.1 mL/min of an aqueous solution of 10 wt% butanol into the reactor, the flow rate of an additional gas through the reactor determines the concentrations of the reactant and water. In particular, at vapor–liquid equilibrium, the addition of a sweep gas leads to vaporization of liquid water and butanol, and the extent of vaporization is determined by the flow rate of the sweep gas. We calculate that all of the liquid water in the reactor will be vaporized at a gas flow rate above approximately 70 $cm^3$(STP)/min, as addressed in more detail below. The activities of the five remaining catalysts were next tested in the absence of liquid water, as the flow rate of the gas through the reactor was varied between 70 and 250 $cm^3$(STP)/min, where higher flow rates lead to lower partial pressures of water vapor. As the gas flow rate was increased, the rate of butene production was observed to increase. The nature of this increase was similar for the five catalysts. Fig. 2 shows the normalized rate (rate at given flow divided by the rate at 200–215 $cm^3$(STP)/min given in Table 1, column 1) versus the gas phase flow through the reactor.

Liquid water was next allowed to contact each of the remaining catalysts by decreasing the gas flow through the reactor below 70 $cm^3$(STP)/min. The rate of butanol dehydration decreased for flow rates below 70 $cm^3$(STP)/min for both USY and H-ZSM-5. Upon returning to a higher flow rate (200 $cm^3$(STP)/min), both USY and H-ZSM-5 showed a sharp decrease in activity, as shown in Table 1, column 2. Exposure of these catalysts to liquid water thus led to deactivation, and these two catalysts were not studied further.

The remaining three catalysts demonstrated an increase in activity when liquid water was present. SiAl showed a modest increase in activity from 153 to 181 μmol/g/min, while $Nb_2O_5$ and $NbOPO_4$ both showed significant increases, 40 to 147 and 81 to 262 μmol/g/min, respectively. Moreover, the rates were observed to increase sharply at lower flow rates of gas through the reactor. Upon returning to higher gas flow rates (under conditions leading to complete vaporization of water), a higher rate of butanol dehydration was observed for each of the three catalysts (see Fig. 3).

The acid site density calculated from ammonia TPD, the ratio of the Brønsted/Lewis areas from pyridine IR, and the BET surface area for each catalyst are given in columns 3 through 5 of Table 1. Further studies were performed for the three catalysts that showed an increase in activity after contact with liquid water. These catalysts were treated with water as described in the experimental section. The acid site density, Brønsted/Lewis ratio and BET surface area after this treatment are also given as the second number in columns 3 through 5.

## 3. Discussion

### 3.1. Liquid water/water vapor equilibrium

The vapor pressures of water and 2-butanol at 513 K are 32.9 and 30.4 atm, respectively. With a total system pressure of 52 atm, and in the absence of a flowing gas, water should remain as a liquid. However, if a gas is bubbled through the water, the gas bubbles will carry water vapor through and out of the reactor. At the reaction conditions of this study, the butene produced by the dehydration reaction is present only in the gas phase. Therefore the rate of butene production will also cause the sparging of liquid water. If no butene is formed, then all of the 2-butanol and water are sparged into the gas phase at a gas flow ($F^g_{He}$) through the reactor of 74 $cm^3$(STP)/min. As a second limit, one can consider the case where all the 2-butanol is converted to butene. Under these conditions, a flow of only 68 $cm^3$(STP)/min of inert gas is necessary to vaporize all the water present. Thus, regardless of the reactivity of a catalyst, liquid water will always be present for a gas flow below 68 $cm^3$(STP)/min, and the liquid feeds of 2-butanol and water will be completely vaporized at a gas flow above 74 $cm^3$(STP)/min.

A more quantitative description of the extents of vaporization of water and butanol can be determined from thermodynamic expressions for species in vapor–liquid equilibrium. Literature sources [13] indicate that dilute solutions of butanol in water behave nonideally. The partial pressures, $P_i$, of vapor phase species are given by Eq. (1).

$$P_i = x_i \gamma_i P_i^{Vap} = y_i P_{tot}. \quad (1)$$

In this equation $x_i$ and $y_i$ are mole fractions in the liquid and vapor phases respectively, and $\gamma_i$ are activity coefficients. Substituting Eq. (1) into an expression for the total system pressure results in Eq. (2). The saturation pressures can be obtained from the Antoinne equation using the appropriate constants for each species.

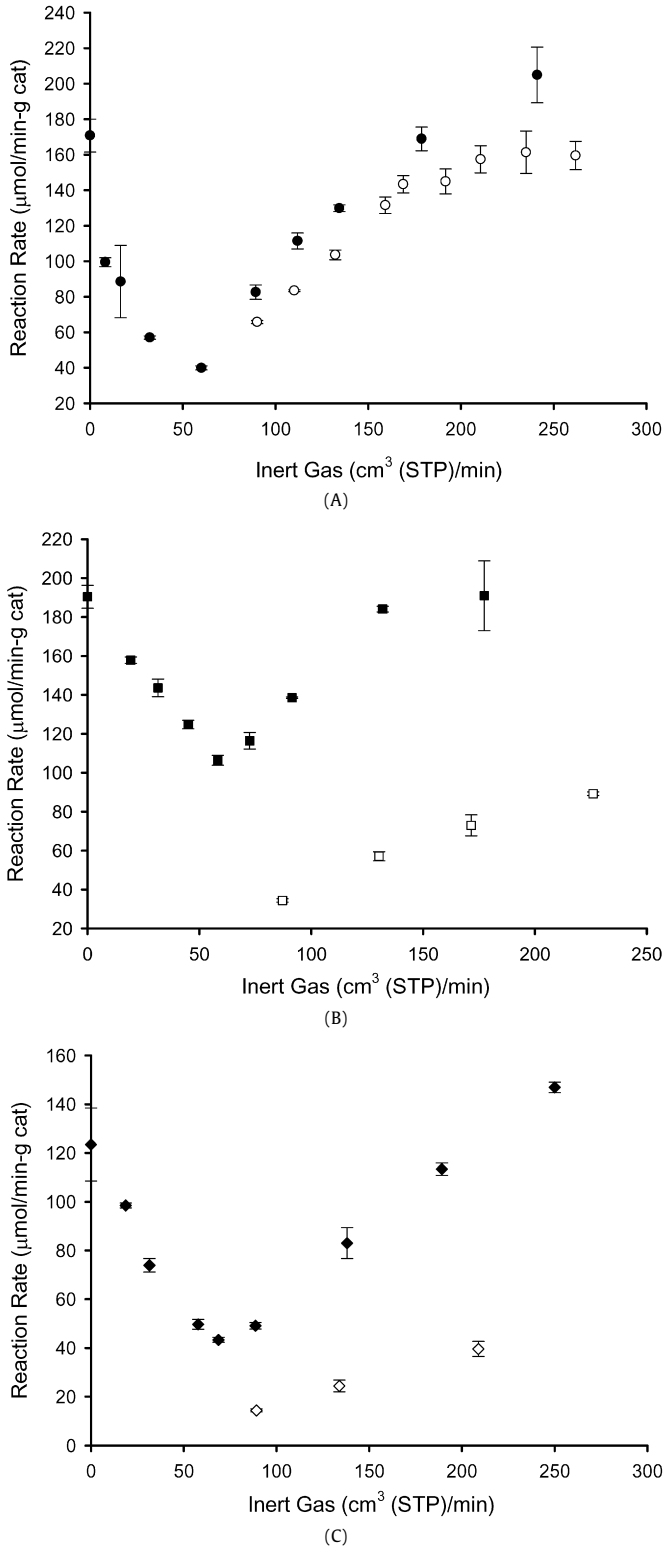


**Fig. 3.** (A) Rate of 2-butanol dehydration versus inert flow rate over SiAl. Initial activity (○); after exposure to liquid water (●). (B) Rate of 2-butanol dehydration versus inert flow rate over $NbOPO_4$. Initial activity (□); after exposure to liquid water (■). (C) Rate of 2-butanol dehydration versus inert flow rate over $Nb_2O_5$. Initial activity (◇); after exposure to liquid water (◆).

$$P_{\text{tot}} = \sum_s P_s = x_{\text{butanol}}\gamma_{\text{butanol}}P^{\text{Sat}}_{\text{butanol}} + (1 - x_{\text{butanol}})\gamma_{\text{water}}P^{\text{Sat}}_{\text{water}} + \frac{P_{\text{tot}}}{F_{\text{tot,gas}}}(F_{\text{butene}} + F_{\text{helium}}). \quad (2)$$

In the expression for the total pressure of the system, Eq. (2), the total flow rate of the vapor phase, $F_{\text{tot,gas}}$, is given by:

$$F_{\text{tot,gas}} = F_{\text{helium}} + F_{\text{butene}} + F_{\text{water,gas}} + F_{\text{butanol,gas}}. \quad (3)$$

While the helium and butene species are present only in the vapor phase, butanol and water are in equilibrium with the liquid and vapor phases. Using the vapor–liquid equilibrium expression for butanol, it is possible to express the total flow rate of butanol in the system as Eq. (4).

$$F_{\text{butanol,tot}} = F_{\text{butanol,gas}} + F_{\text{butanol,liq}} = \frac{x_{\text{butanol}}\gamma_{\text{butanol}}P^{\text{Vap}}_{\text{butanol}}}{(1 - x_{\text{butanol}})\gamma_{\text{water}}P^{\text{Vap}}_{\text{water}}}(F_{\text{water,tot}} - F_{\text{water,liq}}) + \frac{x_{\text{butanol}}}{(1 - x_{\text{butanol}})}F_{\text{water,liq}}. \quad (4)$$

Using Eqs. (2) and (4), the two unknown variables $F_{\text{water,liq}}$ and $x_{\text{butanol}}$ can be determined, and these two variables are then used to calculate $F_{\text{butanol,liq}}$. It is then possible to calculate $F_{\text{water,gas}}$ and $F_{\text{butanol,gas}}$ in terms of $F_{\text{water,tot}}$ and $F_{\text{butanol,tot}}$, and the overall materials balances are then written in terms of these two latter quantities.

The initial values for the activity coefficients for the butanol and water were chosen based on literature [13] as well as numerical simulation of the binary mixture using Aspen. It has been reported that as the mole fraction of butanol in water approaches zero, the activity coefficient for butanol increases significantly. For the mole fractions of butanol used in the current reaction system, approximately 0.03, an activity coefficient of at least 20 is expected for the vapor–liquid regime. Increasing the activity beyond 20 did not have a significant effect on model results, and hence a value of 20 was used for all subsequent calculations. The activity coefficient of water is close to one at the given reaction conditions, and is assumed to be one for the model calculations. Additionally for all model calculations, vapor liquid equilibrium is assumed for all points within the reactor; hence the activities of liquid and gaseous species are the same.

### 3.2. Catalyst performance

SiAl, $NbOPO_4$ and $Nb_2O_5$ all showed high catalytic activity and stability throughout the course of reaction kinetics studies. Importantly, these catalysts did not deactivate after exposure to liquid water, and in fact, the activities of all three catalysts increased after the introduction of liquid water, with $Nb_2O_5$ increasing to the greatest extent (270% increase) followed by $NbOPO_4$ (220% increase) and SiAl (18%). To understand the origin of this increase, the catalysts were characterized before and after treatment with liquid water under high temperature and pressure in a Parr reactor as shown in Table 1. The SiAl catalyst showed a modest increase of about 30% in concentration of acid sites per gram, as measured by ammonia TPD. The $NbOPO_4$ catalyst showed a large increase of 100%, while $Nb_2O_5$ showed an 84% decrease in acid sites concentration. All three catalysts showed a decrease in surface area upon treatment with liquid water. SiAl and $NbOPO_4$ showed modest decreases in surface area of 66% and 54% respectively. $Nb_2O_5$ showed a large decrease in surface area of 86%. For $Nb_2O_5$, the decrease in acid sites concentration (84%) is attributed to the large decrease in surface area under the conditions of this water treatment (86%).

For SiAl the rate increased approximately 20% after treatment in liquid water. From Fig. 3A, it is clear that this rate increase occurred at all gas flows. Water treatment of SiAl increased the acid surface site density by 30% and shifted the ratio of Brønsted/Lewis acids from 0.15 to 12. Because Brønsted acid sites are significantly more active sites for dehydration [7], it appears that the increase in

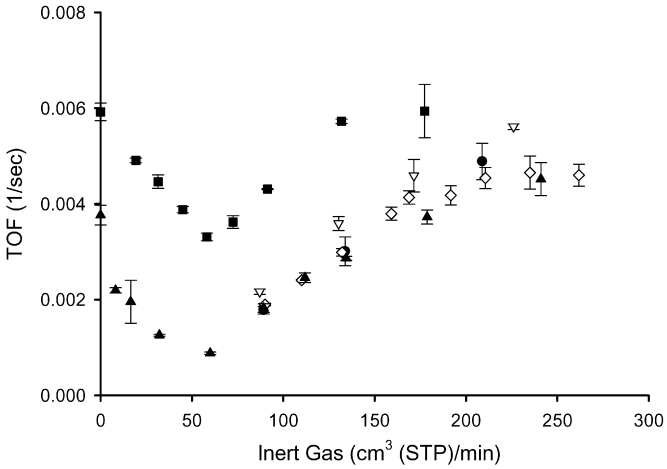


**Fig. 4.** Butene TOF versus inert flow rate. SiAl initial activity (◇); SiAl post liquid water exposure (▲); $NbOPO_4$ initial activity (▽); $NbOPO_4$ post liquid water exposure (■); $Nb_2O_5$ initial activity (●).

**Table 2**
Simple four step surface reaction mechanism.

| Steps | Surface reactions |
|---|---|
| 1. | $C_4H_9OH + * \rightleftarrows C_4H_9OH^*$ |
| 2. | $C_4H_9OH^* + * \rightarrow C_4H_8^* + H_2O^*$ |
| 3. | $C_4H_8 + * \rightleftarrows C_4H_8^*$ |
| 4. | $H_2O + * \rightleftarrows H_2O^*$ |

catalytic activity of SiAl upon treatment with liquid water is caused by an increase in the surface concentration of Brønsted acid sites.

$NbOPO_4$ showed a large increase in both catalytic activity (increase of 220%) and a large increase in the density of surface acid sites (increase of 100%) upon contact with liquid water, see Fig. 3B. The ratio of Brønsted/Lewis area after this treatment remained about constant. Thus, the increase in catalytic activity of $NbOPO_4$ upon treatment with liquid water is again caused primarily by an increase in the surface concentration of Brønsted acid sites. The reactivity change upon exposure to liquid water for $Nb_2O_5$ is similar to that for $NbOPO_4$, and we again suggest that the surface chemistry is controlled by the number of Brønsted acid sites. Fig. 4 shows the rates reported as turnover frequencies. It is clear from Fig. 4 that the TOF values are similar for all catalysts before water treatment. The TOF values for SiAl are similar after water treatment, whereas $NbOPO_4$ appears to show a modest increase in TOF after water treatment.

### 3.3. Kinetic model formulation

Two adsorption models were used to understand how the flow rate of inert gas through the reactor influences the rates of dehydration in the water-stable systems of SiAl and $NbOPO_4$. The first mechanism is a Langmuir–Hinshelwood (L–H) mechanism and involves the surface reaction of adsorbed butanol with a vacant site to form adsorbed butene and water. Table 2 shows the 4 step simple mechanism. Steps (1), (3), and (4) are the adsorption–desorption steps of butanol, butene, and water, respectively. Step (2) is the surface reaction where the dehydration of butanol occurs. The adsorption–desorption steps are assumed to be quasi-equilibrated. Following L–H kinetics, the surface coverage of species and forward rate are as follows:

$$\theta_{buOH} = K_{buOH} P_{buOH} \theta_v, \tag{5}$$

$$\theta_{butene} = K_{butene} P_{butene} \theta_v, \tag{6}$$

$$\theta_{H_2O} = K_{H_2O} P_{H_2O} \theta_v, \tag{7}$$

$$\theta_v = \frac{1}{[1 + K_{buOH} P_{buOH} + K_{H_2O} P_{H_2O} + K_{butene} P_{butene}]}, \tag{8}$$

$$\text{rate} = \frac{K_{buOH} k_{f,surf.rxn.} P_{buOH} \left(1 - \frac{P_{butene} P_{H_2O}}{P_{buOH} K_{eq}}\right)}{[1 + K_{buOH} P_{buOH} + K_{butene} P_{butene} + K_{H_2O} P_{H_2O}]^2}. \tag{9}$$

The second mechanism examined incorporates multi-layer adsorption of water on the catalyst. The derivation of the multilayer water adsorption coverage is based on the BET adsorption isotherm, as outlined below. The fractional coverage for the first adsorbed water molecule on the catalyst surface can be written as Eq. (10) for quasi-equilibrated adsorption. In this equation $K_{H_2O}$ is the equilibrium constant for the adsorption of water onto the catalyst surface and $\theta_{H_2O}$ is the fractional coverage of mono-adsorbed water. The fractional coverage of a two-water stack on the site can be written as Eq. (11), where $K_{W1}$ is the equilibrium constant for the adsorption of water on an already adsorbed water molecule. The $K_{W1}$ parameter corresponds to the equilibrium constant for liquefaction of water and is set as the inverse of the saturation pressure of water at the reaction temperature. Similarly, the fractional coverage of an $n$-layer stack of water molecules can be written in the form of Eq. (12).

$$\theta_{H_2O} = K_{H_2O} P_{H_2O} \theta_v, \tag{10}$$

$$\theta_{(H_2O)_2} = K_{H_2O} P_{H_2O} K_{W1} P_{H_2O} \theta_v, \tag{11}$$

$$\theta_{(H_2O)_n} = K_{H_2O} P_{H_2O} (K_{W1} P_{H_2O})^{n-1} \theta_v. \tag{12}$$

According to the BET adsorption isotherm, water can adsorb in an infinite number of layers. Equation (13) shows the site balance, where the sum of all species ranges from values of $n$ from 1 to infinity, leading to a geometric Maclaurin series. The repeated term raised to a power in the Maclaurin series is equal to the equilibrium constant for the water liquefaction multiplied by the partial pressure of water.

$$\begin{aligned} 1 &= \theta_v + K_{H_2O} P_{H_2O} \theta_v + K_{H_2O} P_{H_2O} K_{W1} P_{H_2O} \theta_v \\ &\quad + K_{H_2O} P_{H_2O} (K_{W1} P_{H_2O})^2 \theta_v \\ &\quad + \cdots + K_{H_2O} P_{H_2O} (K_{W1} P_{H_2O})^n \theta_v, \\ 1 &= \theta_v \left(1 + \frac{K_{H_2O} P_{H_2O}}{1 - \alpha}\right), \quad \alpha = K_{W1} P_{H_2O}. \end{aligned} \tag{13}$$

A similar approach can be used to derive expressions for the hydration of butanol adsorbed on the surface. In this case, we include butanol adsorbed on dry sites, with equilibrium constant equal to $K_{buOH}$, and we include adsorption of water onto an adsorbed butanol molecule, with an equilibrium constant equal to as $K_{W2}$. The value of $K_{W2}$ can be set equal to the constant of liquefaction, $K_{W1}$, or it can be an adjustable parameter. The resulting fractional surface coverages for adsorbed butanol on a dry site, $\theta_{buOH}$, multilayer water adsorption, $\theta_{hyd}$, and multilayer water adsorption on butanol, $\theta_{buOH\_hyd}$, are shown below.

$$\theta_{butanol} = K_{buOH} P_{buOH} \theta_v, \tag{14}$$

$$\theta_{hyd} = \frac{K_{H_2O} P_{H_2O} \theta_v}{(1 - \alpha)}, \tag{15}$$

$$\theta_{buOH\_hyd} = \frac{K_{buOH} P_{buOH} K_{W2} P_{H_2O} \theta_v}{(1 - \alpha)}, \tag{16}$$

$$\theta_v = \frac{1}{\left[1 + K_{buOH} P_{buOH} + \frac{K_{H_2O} P_{H_2O} + K_{buOH} P_{buOH} K_{W2} P_{H_2O}}{(1-\alpha)}\right]}. \tag{17}$$

The standard state (i.e., 1 atm and 298 K) entropy and enthalpy values are obtained from standard handbooks. The constant pressure heat capacities are used to adjust the enthalpies

and enthalpies to the reaction temperature. The gas phase three-dimensional entropies are calculated for all species using the relation:

$$S^{o}_{\mathrm{trans,3D}} = R\left[\ln\left(\frac{(2\pi m k_B T)^{3/2}}{h^3}\right) + \ln\left[\frac{k_B T}{h}\right] + \frac{5}{2}\right] \quad (18)$$

where $m$ is the mass of the molecule of interest, $h$ is Plank's constant, $k_B$ is Boltzmann's constant and $T$ is the temperature in Kelvin. The thermodynamic properties of the surface species are then determined by adjusting the gas phase thermodynamics accordingly. The enthalpy of formation of an adsorbed species is calculated by adding the binding energy of the molecule to its gas phase enthalpy. The local entropy values (i.e., rotational and vibrational entropies) of the adsorbed species are calculated by subtracting the three-dimensional translational entropy from the gas phase entropy. It is assumed that all of the local entropy was retained by the adsorbed species.

The overall equilibrium constant for each step is calculated from the change in enthalpy and entropy upon reaction. Each equilibrium constant is calculated using Eq. (19).

$$K_{i,\mathrm{eq}} = \exp\left(\frac{-\Delta H^{o}_{i}}{RT} + \frac{\Delta S^{o}_{i}}{R}\right). \quad (19)$$

In this equation, $\Delta H^{o}_{i}$ and $\Delta S^{o}_{i}$ are the change in enthalpy and change in entropy, respectively, for reaction $i$. To ensure thermodynamic consistency, we adjust the forward rate constant to fit the experimental data, and the reverse rate constant is calculated using the expression:

$$k_{i,\mathrm{rev}} = \frac{k_{i,\mathrm{for}}}{K_{i,\mathrm{eq}}}, \quad (20)$$

where $k_{i,\mathrm{for}}$ and $k_{i,\mathrm{rev}}$ are the forward and reverse rate constants, respectively. The binding energies of various species to the surface are taken as adjustable parameters. The specific species under consideration depends upon the type of adsorption and allowed surface reactions as discussed below.

The rate constants for the surface reactions are calculated from the Arrhenius expression in Eq. (21),

$$k_i = A\exp\left(\frac{-E_i}{RT}\right) \quad (21)$$

where $A$ is the pre-exponential factor and $E_i$ is the activation energy barrier in the forward direction. The pre-exponential factors are assumed for simplicity to be equal to the normal value of $10^{13}$ $s^{-1}$ for adsorbed species reacting on a surface. Therefore, the surface reactions are parameterized by the forward activation energy barrier for each respective step.

The initial step in developing the kinetic model is to determine the sensitivity of the parameters to be estimated. The sensitivity is calculated by increasing the model parameter, $P$, by 1% and recording the effect on the overall rate, $r$, for the reaction. The effect on the rate is then normalized by the initial rate and initial parameter value according to equation

$$\sigma_p = \frac{\Delta r}{\Delta P}\frac{P_0}{r_0} \quad (22)$$

where $\Delta r$ and $\Delta P$ are the change in rate and change in parameter value, respectively and $r_0$ and $P_0$ are the initial values for the reaction rate and parameter, respectively. In all cases, the binding energy for butene is found to be insensitive.

The kinetic models are fit to the experimental observations using Matlab software. The model solves a differential equation for the change in butanol flow rate as a function of the length of a packed bed plug flow reactor. The model also includes the algebraic equations to calculate the catalyst surface coverage by adsorbed species as a function of reactor length. The reaction kinetics data for the SiAl and $NbOPO_4$ catalysts (after exposure to liquid water) are then used to fit the catalyst specific parameters for the binding energy of water, binding energy of butanol, activation energies of the surface reactions and the energy for hydration of surface adsorbed butanol. The parameter estimation is performed in Matlab using the nonlinear parameter estimation function 'nlinfit'. The nlinfit function uses the Gauss–Newton algorithm with Levenberg–Marquardt modifications for determining the optimum parameters for the model fit. The nonlinear fitting algorithm uses the butene flow rate out of the reactor for comparing the experimental data with the predicted values. Following the successful convergence of the nonlinear parameter estimation function, the residuals and Jacobian are then used to determine the confidence intervals for the parameters using the 'nlparci' function built into Matlab, which calculates the confidence intervals using a statistical method based on the asymptotic normal distribution for the parameters estimates. Two adsorption schemes and multiple reaction schemes are considered. A summary of the schemes that predict the correct trends is given in Table 3. The individual entries in the table are discussed below.

**Table 3**
Summary of reaction schemes for butanol dehydration.

| Entry | Adsorption | Surface reactions | Parameters | # Par. |
|---|---|---|---|---|
| 1 | L–H | $buOH^* + * \rightarrow$ | $Ea_1$, $BE_{buOH}$, $BE_{H_2O}$ | 3 |
| 2 | Multilayer | $buOH^* + * \rightarrow$ | $Ea_1$, $BE_{buOH}$, $BE_{H_2O}$ | 4 |
| | | $buOHhyd^* + hyd^* \rightarrow$ | $Ea_2$ | |
| 3 | Multilayer | $buOH^* + * \rightarrow$ | $Ea_1$, $BE_{buOH}$, $BE_{H_2O}$ | 5 |
| | | $buOHhyd^* + hyd^* \rightarrow$ | $Ea_2$ | |
| | | $buOH^* + hyd^* \rightarrow$ | $Ea_3$ | |
| 4 | Multilayer | $buOH^* + * \rightarrow$ | $Ea_1$, $BE_{buOH}$, $BE_{H_2O}$ | 5 |
| | | $buOHhyd^* + hyd^* \rightarrow$ | $Ea_2$, $BE_{buOH-H_2O}$ | |
| 5 | Multilayer | $buOH^* + * \rightarrow$ | $Ea_1$, $BE_{buOH}$, $BE_{H_2O}$ | 6 |
| | | $buOHhyd^* + hyd^* \rightarrow$ | $Ea_2$, $BE_{buOH-H_2O}$ | |
| | | $buOH^* + hyd^* \rightarrow$ | $Ea_3$ | |

### 3.4. Kinetic model results

The simple Langmuir–Hinshelwood mechanism involves fitting 3 parameters: the activation energy of reaction, $Ea_1$, and the binding energies of butanol and water, $BE_{buOH}$, and $BE_{H_2O}$ (Table 3, Entry 1). The best fit for this model does not accurately predict the behavior of the liquid/water system, as shown in Fig. 5 for SiAl and $NbOPO_4$. The general trend of increasing rate at gas flow rates above and below 70 $cm^3$(STP)/min of inert flow is predicted qualitatively. At gas flow rates above 70 $cm^3$(STP)/min, increased inert gas flow decreases the partial pressure of water, thus increasing the rate. However, the effect of the changing partial pressures of reactants was not sufficiently pronounced in the simple mechanism to predict the rates at high inert flow. At gas flow rates below 70 $cm^3$(STP)/min, the non-ideality of the butanol water system, as incorporated by the butanol activity coefficient, predicts that the rate will decrease with increasing gas flow rate. In this range of gas flow rates where liquid water is present in the reactor, increasing the gas flow rate leads to the preferential vaporization of butanol because of the high value of the activity coefficient. In particular, molar flow rates of butanol and water in the gas and liquid phases are given by:

$$\frac{F_{buOH,gas}}{F_{H_2O,gas}} = \frac{x_{buOH}\gamma_{buOH}P_{buOH}}{(1-x_{buOH})P_{H_2O}},$$

$$\frac{F_{buOH,liq}}{F_{H_2O,liq}} = \frac{x_{buOH}}{(1-x_{buOH})},$$

and because the value of $\gamma_{buOH}P_{buOH}/P_{H_2O}$ is greater than 1 ($\gamma_{buOH} = 20$), the composition of the vapor phase is enriched in butanol compared to the composition of the liquid phase. Thus,

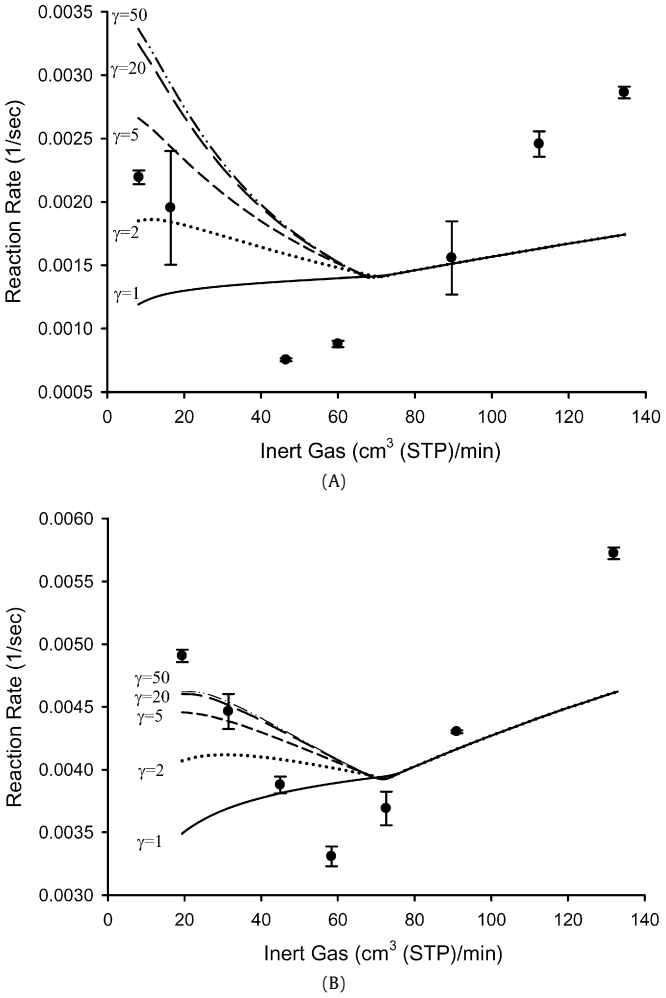


**Fig. 5.** (A) Experimental data (●) for 2-butanol dehydration over SiAl modeled with Langmuir–Hinshelwood mechanism at varying activity coefficients. (B) Experimental data (●) for 2-butanol dehydration over $NbOPO_4$ modeled with Langmuir–Hinshelwood mechanism at varying activity coefficients.

the partial pressure of butanol in the reactor decreases with an increase in the gas flow rate, as shown in Fig. 6, while the partial pressure of water remains constant provided that all of the liquid water is not vaporized. Increasing the activity coefficient beyond a value of 20 does not significantly impact the model as shown in Fig. 5 for SiAl and $NbOPO_4$.

For the multilayer adsorption model, there are multiple surface reactions and multiple binding energies that can be modeled when considering the different surface species present on the catalyst, including the reaction of butanol, or hydrated butanol, with vacant sites, hydrated sites or with both. The butanol and water binding energies with the surface are included in every model. Additionally in some models, the binding energy of water on butanol is allowed to vary from its initial set value, the heat of liquefaction of water.

The simplest surface reaction scheme involves the L–H mechanism previously described, where adsorbed butanol reacts with a vacant site to produce adsorbed butene and water. This reaction mechanism fails to describe the experimental data for all multilayered adsorption simulations. In this scheme a vacant site is necessary for reaction, and there are no vacant sites in the liquid water regime due to the multilayered adsorption of water on the surface.

If a second surface reaction step for reaction is included, the multilayered adsorption correctly predicts the trends seen in experiments (Table 3, Entry 2). In this model, a hydrated site can also

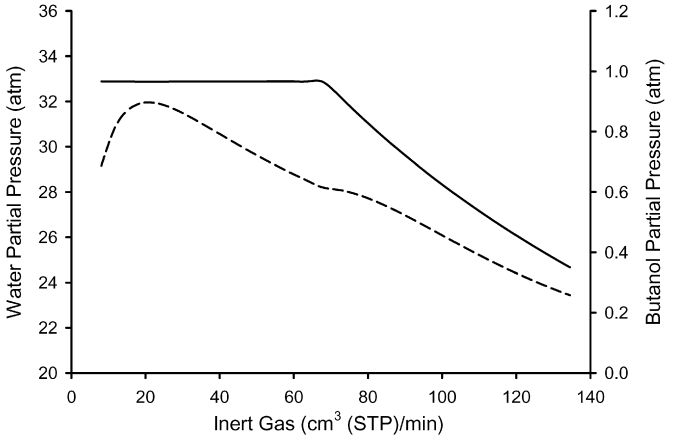


**Fig. 6.** Calculated partial pressures at the outlet of the reactor for water (solid line) and butanol (dashed line) under reactive conditions as a function of inert gas flow.

react with adsorbed–hydrated butanol to form butene and water. The addition of this step adds an additional parameter, namely the activation energy of this second surface reaction. The reaction of butanol (without water adsorbed on it) with a hydrated site, however, fails to predict the experimentally observed trends.

The addition of a third surface reaction to the model also predicts the correct trends. The three surface reactions are adsorbed butanol with a vacant site, adsorbed butanol with a hydrated site, and adsorbed–hydrated butanol with a hydrated site (Table 3, Entry 3). The addition of this third reaction adds a third activation energy as an adjustable parameter to the model.

The final adjustable parameter under consideration is the binding energy of water on adsorbed butanol. In Entries 2 and 3 of Table 3, this binding energy was constant. Entry 4 in Table 3 uses the same two surface reaction steps as Entry 2; however, the binding energy of water on butanol is adjustable. Likewise, Entry 5 uses the same three surface reaction steps as Entry 3, with the binding energy of water on butanol being adjustable.

To determine the model that best fits the experimental observations with the minimum number of parameters, the Akaike Information Criterion (AIC) is calculated for each proposed variation of the multilayer adsorption model [14]. The AIC is calculated using the second order equation

$$\mathrm{AICc} = \mathrm{AIC} + \frac{2k(k+1)}{n-k-1}, \tag{23}$$

$$\mathrm{AIC} = 2k + n\left[\ln\left(\frac{2\pi\,\mathrm{RSS}}{n}\right) + 1\right], \tag{24}$$

where $k$ is the number of parameters, $n$ is the number of observations and RSS is the residual sum of squares. The best model corresponds to the minimum value of AICc. This analysis indicates that the model that best fits the experimental observations with the minimum number of parameters contains only two surface reactions, the reaction between a monolayer adsorbed butanol and a vacant site, and the reaction between a butanol molecule that has multiple layers of water adsorbed with a catalyst site that has multiple layers of water adsorbed (Table 3, Entry 2). The model fit for SiAl and $NbOPO_4$ can be seen in Fig. 7, while a graph for the AIC analysis is shown in Fig. 8.

The optimized parameter values and corresponding confidence intervals for the best model are shown in Table 4, column 1. The confidence intervals are within a few percent of the parameter value and are in good agreement between the two catalysts tested, $NbOPO_4$ and SiAl.

A plot of the predicted catalyst coverage as a function of helium flow rate is shown in Fig. 9. In the regime containing liquid

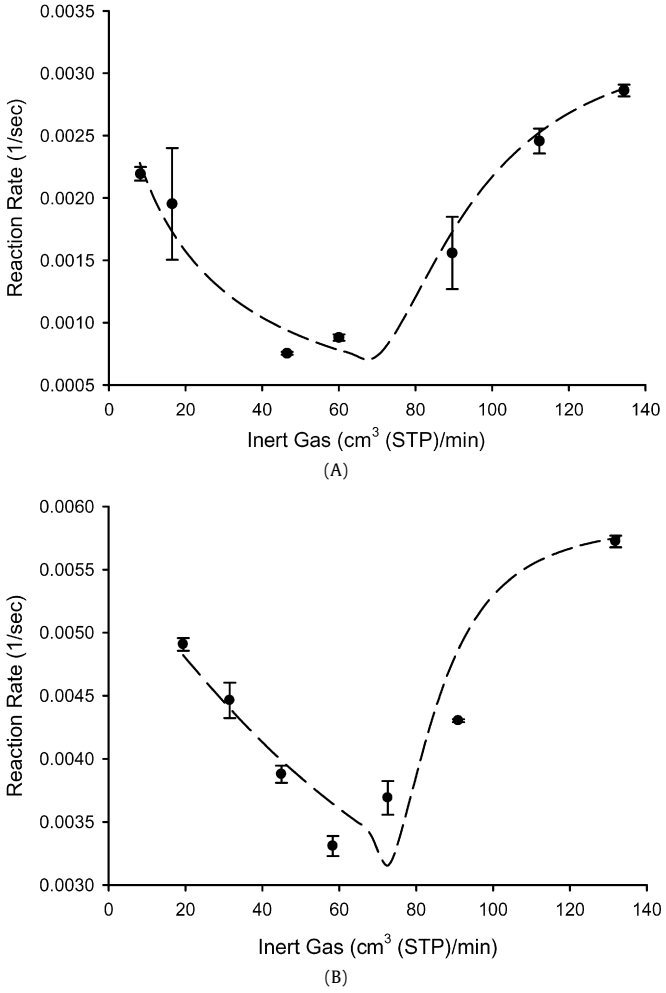


**Fig. 7.** (A) Model fit (dashed line) for BET multilayer adsorption mechanism with 2 surface reactions for 2-butanol dehydration over SiAl (●). (B) Model fit (dashed line) for BET multilayer adsorption mechanism with 2 surface reactions for 2-butanol dehydration over $NbOPO_4$ (●).

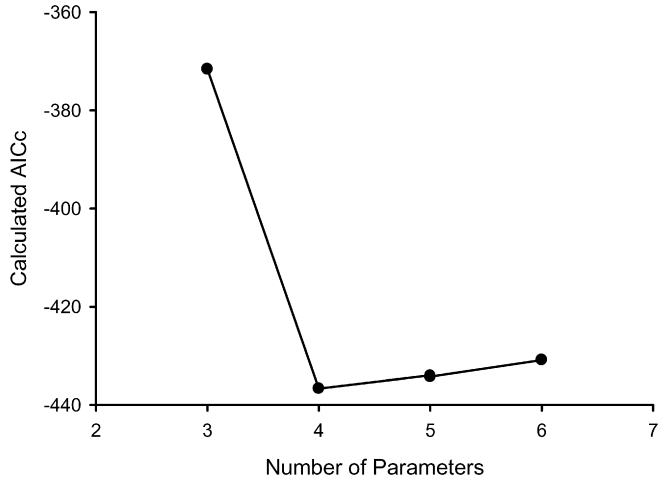


**Fig. 8.** Akaike Information Criterion calculated values (●) for proposed reaction mechanisms.

water, the dominant species predicted for the model is the multilayer adsorbed water species, with a small fraction of adsorbed butanol with multiple layers of adsorbed water. In the vapor-only regime, the fraction of vacant sites is predicted to increase from a negligible amount to approximately 60% vacancy over the range

**Table 4**
Optimized kinetic and thermodynamic parameters with corresponding 95% confidence intervals.

| | Varied inert gas flow (kJ/mol)[a] | Varied water vapor (kJ/mol)[a] |
|---|---|---|
| $NbOPO_4$ | | |
| $Ea_1$ | $127 \pm 4$ | |
| $Ea_2$ | $144 \pm 1$ | |
| $BE_{buOH}$ | $-76 \pm 2$ | |
| $BE_{H_2O}$ | $-56 \pm 2$ | |
| SiAl | | |
| $Ea_1$ | $125 \pm 5$ | $118 \pm 48$ |
| $Ea_2$ | $144 \pm 4$ | $135 \pm 48$ |
| $BE_{buOH}$ | $-70 \pm 5$ | $-70 \pm 49$ |
| $BE_{H_2O}$ | $-59 \pm 1$ | $-66 \pm 1$ |

[a] ±95% confidence interval.

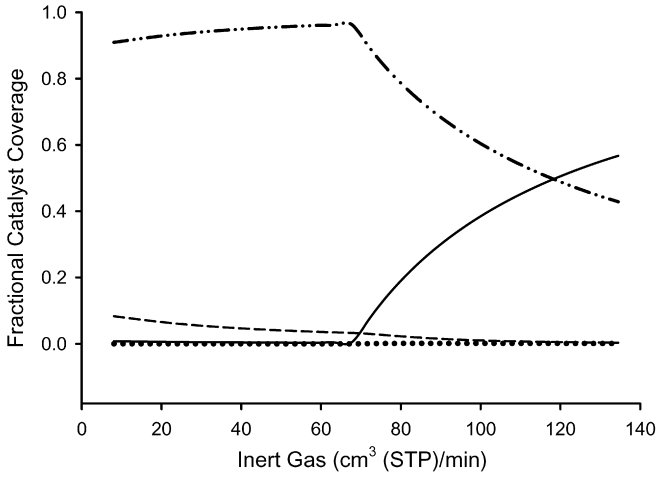


**Fig. 9.** Calculated fractional surface coverage for SiAl data: vacant sites, $\theta_v$ (solid line); mono-adsorbed butanol, $\theta_{buOH}$ (dotted line); multilayer water adsorbed on butanol, $\theta_{buOH\,hyd}$ (dashed line); and multilayer adsorbed water, $\theta_{hyd}$ (dash–dot line).

studied. The fraction of multilayer adsorbed water decreases from approximately 95% to almost 40% over the range studied. The surface coverage by butanol species containing multilayers of water is predicted to decrease from 5% to a negligible amount in the vapor-only regime.

The effects of the changing catalyst coverage on the surface reaction rates in the model are shown in Fig. 10. The dominant reaction surface reaction in the liquid water regime is the reaction between an adsorbed–hydrated butanol molecule and a hydrated vacant site. This surface reaction is predicted to decrease steadily with increasing helium sparging. The surface reaction between mono-adsorbed butanol and a vacant site is predicted to be negligible throughout the regime containing liquid water, and it increases significantly in the vapor-only regime.

To test the model further, the flow rate of water and inert were experimentally varied over SiAl such that the total molar flow and butanol flow rate are held constant. The two-reaction multilayered adsorption model is applied to this data set using the previously determined optimized parameters. The resulting model and experimental points can be seen in Fig. 11. The model predictions are in good agreement with the experimental data collected at the varying water molar flow rates. Additionally, the 4 model parameters were readjusted to this new data and are included in the right column of Table 4. The fit values of this second set are just outside the 95% confidence intervals of the previous model for SiAl, however, the 95% confidence intervals for the two models overlap.

The estimated kinetic parameters from Table 4 compare favorably with values found in both experimental and theoretical

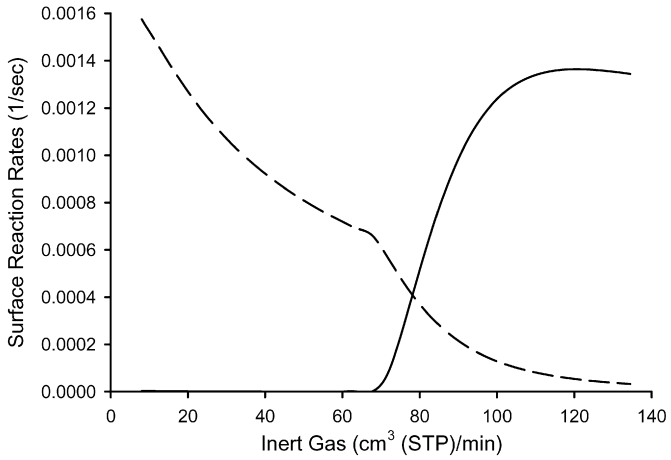


**Fig. 10.** Surface reaction rates for mono-adsorbed butanol with a vacant site (solid line) and surface reaction rate for multilayer water on butanol site with a water multilayer site (dashed line) using the best-fit kinetic model and optimized parameters for $NbOPO_4$.

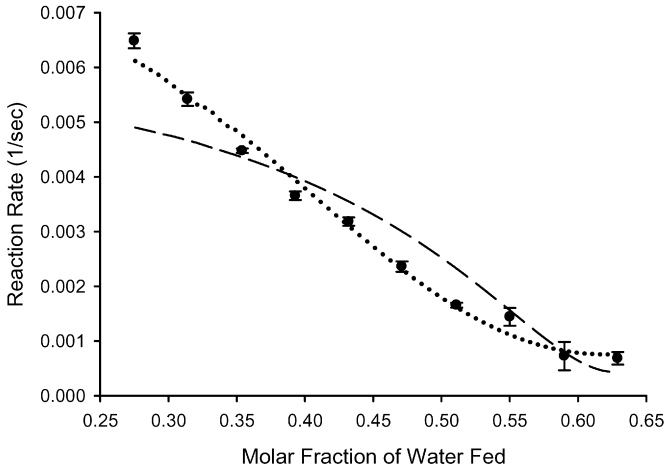


**Fig. 11.** Kinetic model results using the best-fit model for varying molar fraction of water fed over SiAl catalyst. The experimental data (●) are fit using the previously optimized parameters (dashed line) as well as optimized parameters specific to the data set (dotted line).

studies. It is typically observed that the heat of adsorption for a molecule decreases from a relatively high value on a completely dehydrated surface to the enthalpy of liquefaction as the surface becomes saturated with multiple layers of the molecule [15–19]. Therefore, for the current study it is anticipated that the estimated binding energy for water should be between the binding energy on a clean surface and the enthalpy of liquefaction for water. For water binding on the zeolite ZSM-5, the binding energy of water on the proton form, H-ZSM-5 has been reported as $51 \pm 4$ kJ/mol for the binding of one water molecule to one site [20], while the binding to various sodium forms has been reported in the range of 50–60 kJ/mol [15]. Values for water adsorption on amorphous silica-aluminas could not be found; however, values for amorphous silicates are reported as 90–50 kJ/mol [16], 47–49 kJ/mol [17], and 40–53 kJ/mol [18]. These values compare closely to the estimated values for water adsorption of $56 \pm 2$ for $NbOPO_4$ and $59 \pm 2$ or $66 \pm 1$ for SiAl in Table 4.

Reported binding energies for alcohols are comparable to the estimated binding energy for butanol on the catalysts studied. Alcohols such as methanol bind more strongly to acid sites than water [20]. Binding energies from 50–65 kJ/mol [21] and 58–83 kJ/mol ([22] and references therein) have been reported for alcohols on H-ZSM-5. Values for alcohol adsorption on amorphous silica-aluminas could not be found; however, alcohol binding energies on amorphous silicates cover a range of values: 42.8 kJ/mol [19] and 60–67 kJ/mol [18] for methanol; 55 kJ/mol [19] for ethanol; and 67–77 kJ/mol [18] for tert-butyl alcohol. These reported values compare closely to the estimated binding energy for butanol on $NbOPO_4$, $76 \pm 2$ kJ/mol, and on SiAl, $70 \pm 5$ kJ/mol, in Table 4.

The reaction temperature for all experiments performed was held constant at 513 K. Therefore, the activation energies for the surface reactions cannot be distinguished from the pre-exponential factors used. For this reason, absolute comparisons cannot be made between the estimated activation energies and values reported in literature. However, because the same pre-exponential factor is used for all surface reactions in the model, relative comparisons can be made for the differences in the estimated activation energies. The activation energy for the hydrated site reaction ($Ea_2$) is approximately 17 to 19 kJ/mol higher than the corresponding activation energy for the dry site reaction ($Ea_1$). Both theoretical and experimental studies have shown that acidic proton sites can be covered with either one or two water molecules [20,23]. Upon adsorption of a second water molecule, the binding energy per water molecule is decreased by 11–17 kJ/mol; a theoretical study predicted a binding energy decrease from 48 to 37 kJ/mol [23] while an experimental study measured a binding energy decrease from 51 to 34 kJ/mol [20]. Therefore, a hydrated site is expected to bind a species less strongly than a non-hydrated site. Because the apparent activation energy is a sum of the intrinsic activation energy plus the heat of adsorption [24], our observed increase of 17 to 19 kJ/mol in the value of the activation energy ($Ea_2$ vs. $Ea_1$) compares favorably with the expected difference in binding energy of 11 to 17 kJ/mol.

## 4. Conclusions

Under the conditions of this study, we find that SiAl, $NbOPO_4$ and $Nb_2O_5$ are suitable for dehydration of butanol in environments containing high concentrations of water. These three catalysts show increased activity after treatment with liquid water, due to the formation of Brønsted acid sites. The rate of butene production from an aqueous solution of butanol (10 wt%) is strongly influenced by the flow rate of sweep gas through the reactor, due to vaporization of butanol and water. At low flow rates of gas, increasing the gas flow rate causes the preferential vaporization of butanol because of the high activity coefficient of dilute alcohol in water. Above a critical gas flow rate, the liquid feed becomes completely volatilized in the reactor. Increasing the gas flow rate in the complete vaporization regime causes a decrease in the partial pressure of both water and butanol.

Various kinetic models including multilayer adsorption of water on the catalyst surface can be used to describe the experimental observations. These kinetic models are able to seamlessly predict the transition from a completely vaporized regime to a mixed vapor–liquid regime. In the vapor–liquid equilibrium regime the models predict that most of the catalyst is covered with multiple layers of water and dehydration takes place by reaction of hydrated–adsorbed butanol with a hydrated surface site. In the vapor-only regime the model predicts that the fraction of vacant active sites increases with increasing gas flow rate as the fraction of sites covered by multiple layers of water decreases and dehydration takes place by reaction of adsorbed butanol with a vacant surface site.

## Acknowledgments

Supported by U.S. Department of Energy Office of Basic Energy Sciences and the National Science Foundation Chemical and Trans-

port Systems Division of the Directorate for Engineering. We also thank E. Kunkes and E. Codner for technical assistance.

## References

[1] Y. Roman-Leshkov, J.N. Chheda, J.A. Dumesic, Science 312 (2006) 1933.
[2] Y. Roman-Leshkov, C.J. Barrett, Z.Y. Liu, J.A. Dumesic, Nature 447 (2007) 982.
[3] G.W. Huber, R.D. Cortright, J.A. Dumesic, Angew. Chem. Int. Ed. 43 (2004) 1549.
[4] R.M. West, Z.Y. Liu, M. Peter, J.A. Dumesic, ChemSusChem 1 (2008) 417.
[5] E.L. Kunkes, D.A. Simonetti, R.M. West, J.C. Serrano-Ruiz, C.A. Gärtner, J.A. Dumesic, Science 322 (2008) 417.
[6] L. Li, Y. Yoshinaga, T. Okuhara, Phys. Chem. Chem. Phys. 4 (2002) 6129.
[7] C.D. Baertsch, K.T. Komala, Y.H. Chua, E. Inglesia, J. Catal. 205 (2002) 44.
[8] M.A. Sanchez-Castillo, R.J. Madon, J.A. Dumesic, J. Phys. Chem. B 109 (2005) 2164.
[9] H. Liu, P. Cheung, E. Iglesia, J. Phys. Chem. B 107 (2003) 4118.
[10] M.A. Aramendia, V. Borau, C. Jimenez, A. Marinas, J.M. Marinas, J.A. Navio, J.R. Ruiz, F.J. Urbano, Colloids Surf. A 234 (2004) 17.
[11] R.R. Soares, D.A. Simonetti, J.A. Dumesic, Angew. Chem. Int. Ed. 45 (2006) 3982.
[12] N.K. Mal, A. Bhaumik, P. Kumar, M. Fujiwara, Chem. Commun. 7 (2003) 872.
[13] P.G. Whitehead, S.I. Sandler, Fluid Phase Equilib. 157 (1999) 111.
[14] G. Glatting, P. Kletting, S.N. Reske, K. Holm, C. Ring, Med. Phys. 34 (2007) 4285.
[15] K. Tsutsumi, K. Mizoe, Colloids Surf. 37 (1989) 29.
[16] V. Bolis, B. Fubini, L. Marchese, G. Marta, D. Costa, J. Chem. Soc. Faraday Trans. 87 (1991) 497.
[17] E.O. Pedram, A.L. Hines, J. Chem. Eng. 28 (1983) 11.
[18] B. Fubini, V. Bolis, A. Cavenago, E. Garrone, P. Ugliengo, Langmuir 9 (1993) 2712.
[19] B.J. Stanley, G. Guiochon, Langmuir 11 (1995) 1735.
[20] A. Ison, R.J. Gorte, J. Catal. 89 (1984) 150.
[21] B. Hunger, S. Matysik, M. Heuchel, W. Einicke, Langmuir 13 (1997) 6249.
[22] P.E. Sinclair, R.A. Catlow, J. Chem. Soc. Faraday Trans. 93 (1997) 333.
[23] M. Krossner, J. Sauer, J. Phys. Chem. 100 (1996) 6199.
[24] M.I. Temkin, Adv. Catal. (1979) 173.